Hydrothermal synthesis of shape-controlled SnO as anode material for Li-ion batteries

Yayi Cheng, Jianfeng Huang ✉, Jiayin Li, Liyun Cao, Hui Qi

School of Materials Science & Engineering, Shanxi University of Science & Technology, Xi'an 710021, People's Republic of China
✉ *E-mail: huangjfsust@126.com*

Published in Micro & Nano Letters; Received on 3rd August 2017; Revised on 13th October 2017; Accepted on 25th October 2017

The high purity of stannous oxide (SnO) materials with various structures were synthesised using a facile hydrothermal method. Different SnO structures with cross, block, and shell were obtained by controlling pH value and surfactant during the hydrothermal reaction. As anode for lithium-ion batteries (LIBs), the crossed SnO displays superior cycling and rate capability in comparison with the block and shell liked SnO. The difference could be attributed to the special morphology of crossed SnO that shows small particle size, high crystallinity, and good structural stability. All the results suggest that controlling structure is an effective way to improve the electrochemical performances of SnO anode material in LIBs.

1. Introduction: Nowadays, lithium-ion batteries (LIBs) have been widely used as the power source not only in hybrid electric vehicles (EVs), plug-in EVs and EVs, but also in portable electronic devices [1–3], owning to its high energy density, long life cycle and great abundance [4, 5]. To meet the growing demands for high power and high energy of LIBs, many kinds of anode materials have been extensively studied to instead traditional graphitised carbon anode (low theoretical capacity of 372 mAh g^{-1}) [6–8]. Among the anode materials for LIBs, Sn has attracted tremendous attention as one of the most promising candidates due to the high theoretical capacity of 994 mAh g^{-1} [9], which is nearly three times higher than those of commercial graphite anodes. Unfortunately, this high capacity comes at the cost of huge volumetric changes during Li ions insertion and extraction process, leading to pulverisation of electrode and rapid degradation of capacity [10].

Stannous oxide (SnO) is believed to be a potential substitution for Sn anodes. Since the Li_2O formed during the reaction between SnO and Li^+ in the first step, can reduce overall volume expansion and enhance the mechanical robustness of the particle according to the previous report [11, 12]. However, the preparation of SnO is relatively difficult because disproportionation or oxidation of SnO can easily occur [13, 14]. Although several synthetic routes have been reported for the preparation of SnO crystals with different structures, such as wires [15], nanoparticles [16], nanoribbons [17], nanosheets [18–20], nanoplates [21], nanoflowers [22], microspheres [23], diskettes [24], microplates [25] nanoflakes-based self-assembling crossed structures [26], self-assembled nanosquare sheets [27], hierarchical nanocrystals [28] and so forth. There are few works studying about electrochemical behaviours of SnO. As we all know, the morphology and size could affect the electrochemical performance of electrode materials significantly [29–32]. Therefore, it is most essential for us to explore the lithium storage mechanism of SnO with various structures.

In this Letter, we present a facile hydrothermal method for preparation different structures of high pure SnO, including cross, block, and shell-like morphology. The crossed SnO as LIBs anode displays superior cycling and rate capability in comparison with block and shell SnO. The specific reasons have also been discussed in this Letter.

2. Experimental

2.1. Sample preparation: The SnO with various structures were synthesised using a simple hydrothermal method. In a typical synthesis of SnO, 1.128 g $SnCl_2{\cdot}2H_2O$ was dissolved in 50 ml deionised water. Then moderate $NH_3{\cdot}H_2O$ (25–28 wt%) was added to the above solution to reach the desired pH value (pH = 7.5, 10.0, and 11.3, respectively). When the pH value was set at 7.5, additional 2.4 g citric acid was added as a surfactant. After that, the mixture solution with continuously magnetic stirring for 1 h at room temperature was transferred into a 100 mL Teflon-lined stainless steel autoclave filled with N_2 as protection gas, sealed and maintained at 180°C for 4.5 h. After cooling down naturally, the black precipitates were separated by centrifugation and washed five times with deioniser water. Finally, the products, SnO with different structures, were obtained by freeze-drying. The corresponding samples which synthesised by controlling pH value were labelled as SnO-S (pH = 7.5), SnO-C (pH = 10.0), and SnO-B (pH = 11.3), respectively.

2.2. Materials characterisation: X-ray diffraction (XRD) patterns were collected with a Rigaku/max 2200 V diffractometer operating with Cu Kα radiation ($\lambda = 0.15406$ nm) to characterise the chemical composition of samples. The size and microstructures of the as-prepared products were observed by field emission scanning electron microscopy (FESEM, Hitachi, S-4800).

2.3. Cell fabrication and electrochemical measurements: The electrochemical performance of the fabricated SnO with various structures was analysed by constructing 2032-type coin cells in the argon-filled glove box (Braun, Germany). Each electrode was prepared by mixing the active material, sodium carboxymethyl cellulose binder and conductive additive (super P) together in a weight ratio of 8:1:1 in water and pasted on copper foil. Then it was dried as a working electrode in a vacuum oven at 110°C for 24 h. The area of the electrode was about 1.96 cm^2 and the mass of active materials on the electrode was around ~2 mg. Li foil was used as the counter electrode and microporous polypropylene film as the separator. The electrolyte solution was 1 M $LiPF_6$ dissolved in a mixture of ethylene carbonate, ethyl methyl carbonate, and dimethyl carbonate (1:1:1 in volume). The charge–discharge performance of the samples was conducted on a Neware battery testing system at a desired current density with a voltage range of 0.001–2.0 V (versus Li/Li^+). Cyclic voltammetry (CV) was operated using CHI 600D electrochemistry workstation with a scan rate of 0.1 $mV{\cdot}s^{-1}$. Electrochemical impedance

spectroscopy (EIS) results were obtained in a frequency range of 100 kHz–0.01 Hz.

3. Results and discussion: The composition and purity of the as-prepared samples were characterised by XRD. As shown in Fig. 1, SnO-S presents a little impurity of Sn_2O_3 when prepared in neutral solution. The SnO-C and SnO-B synthesised in alkaline solution obtain a high purity of SnO, and all the diffraction peaks can be well indexed to tetragonal SnO phase (JCPDS Card No. 06-0395). With the changing of pH value, the samples display different peak intensity at 29.86°, corresponding to (101) plane. Among them, SnO-C sample shows the strongest intensity in comparison with SnO-B and SnO-S, demonstrating the good crystallinity of the prepared SnO-C. On the contrary, SnO-S has a relatively poor degree of crystallinity. This may have an influence on the electrochemical performances of the SnO.

Fig. 2 shows the scanning electron microscopy (SEM) images of SnO products obtained at different pH value. In Fig. 2*a*, the SnO synthesised at pH = 7.5 (SnO-S) presents shell-like morphology with the particle size around 20 µm. The shell is constructed from the sheet and between the sheets are some nanoparticles (see Fig. 2*b*). Fig. 2*c* reveals the homogeneous crossed structure (SnO-C) with the rough surface and average size is about 6 µm. The typical morphology is evident at higher magnification in Fig. 2*d*, demonstrating that the crossed morphology is assembled by many nanoparticles. When the pH value is controlled at 11.3 (Fig. 2*e*), block-like SnO (SnO-B) particles with cubic shape are obtained. A further observation from Fig. 2*f*, it is found that the block structure is 10–20 µm in width and ~8 µm in thickness. The morphology and particle size have a significant effect on the charge transfer in the electrode.

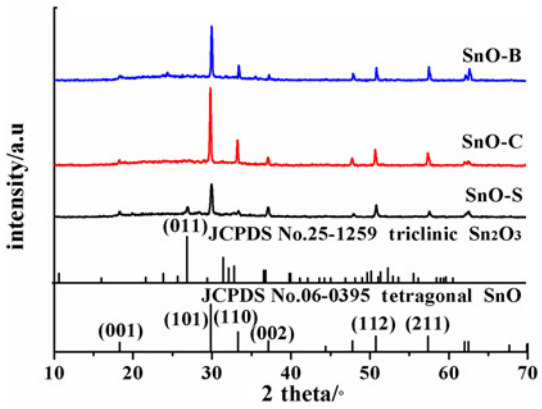

Fig. 1 *XRD patterns of SnO-S (pH = 7.5, 2.4 g citric acid), SnO-C (pH = 10.0), and SnO-B (pH = 11.3)*

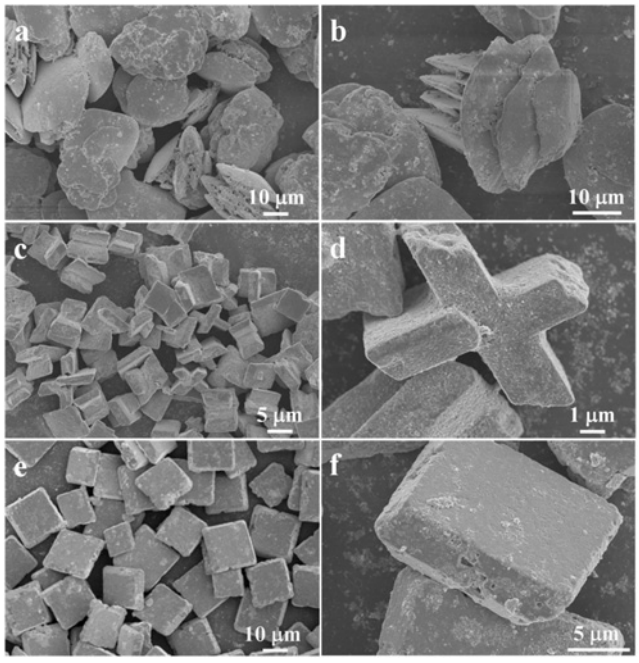

Fig. 2 *SEM images of*
a SnO-S
c SnO-C and
e SnO-B
b, *d*, *f* Show corresponding SEM images at high magnification

Transmission electron microscope (TEM) and high-resolution transmission electron microscopy (HRTEM) measurements were conducted to further examine the structure of the three samples. As shown in Figs. 3*a*, *c* and *e*, the particle size of SnO-S, SnO-C, and SnO-B is about 20, 5, and 15 µm, respectively. The results are well agreement with the SEM. The HRTEM images were observed to confirm the phase of the samples. For SnO-S, in Fig. 3*b*, the calculated space of lattice fringes is about 0.298 and 0.33 nm, which corresponds to the interplanar spacing of SnO (101) plane and Sn_2O_3 (011) plane. In Figs. 3*d* and *f*, the different crystal planes of SnO are well indexed, indicating the high purity of SnO-C and SnO-B. We infer that the SnO with various structures would display different Li storage behaviour.

Cyclic voltammograms (CV) was performed to get a clear insight into the Li-storage mechanism. Figs. 4*a*–*c* show the initial two CV profiles of the SnO-C, SnO-B, and SnO-S at the scan rate of 0.1 mV s^{-1}, respectively. They have similar shapes of CV curves with the reduction peaks locating at ~0.72, ~0.3, and ~0.01 V, the corresponding oxidation peaks at~0.73, ~0.63, ~0.48, and ~0.04 V, respectively. Generally, the cathodic peak at ~0.72 V on the first cycle is associated with the reduction of SnO to Sn, as well as the formation of a solid electrolyte interphase layer on the anode surface. Cathodic peaks ranging from 0.65 to 0.01 V can be attributed to the Li insertion into Sn to form Li_xSn alloys. In the first anodic process, anodic peaks from 0.73 to 0.04 V corresponding to the dealloying reaction of Li_xSn alloy to Sn. The electrochemical reactions of SnO with Li^+ could be ascribed as follows [33, 34]:

$$Li^+ + e^- + \text{electrolyte} \rightarrow \text{SEI}$$

$$SnO + 2Li^+ + 2e^- \rightarrow Sn + Li_2O$$

$$Sn + xLi^+ + xe^- \leftrightarrow Li_xSn$$

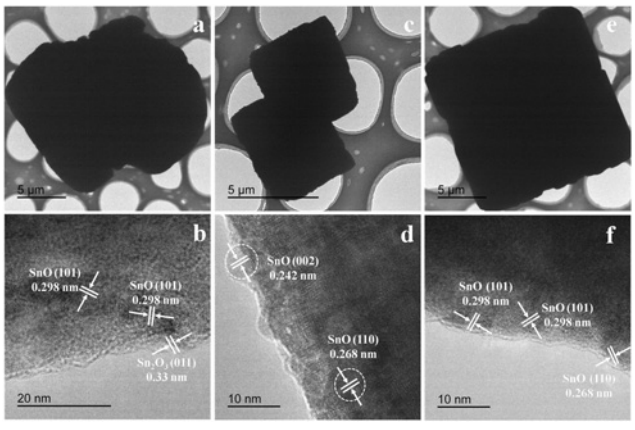

Fig. 3 *TEM and corresponding HRTEM images of*
a, *b* SnO-S
c, *d* SnO-C and
e, *f* SnO-B

doi: 10.1049/mnl.2017.0550

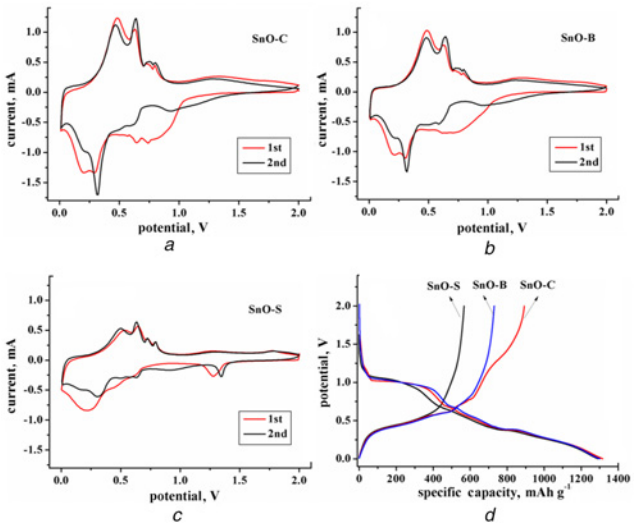

Fig. 4 *CV of*
a SnO-C
b SnO-B and
c SnO-S in the first and second cycles
d Initial discharge–charge profiles of SnO-C, SnO-B, and SnO-S at the current density of 50 mA g^{-1}

In addition, SnO-C electrode shows a larger integral area of CV profiles in comparison with the SnO-B and SnO-S electrodes, indicating that SnO-C could deliver higher capacity. As shown in Fig. 3*d*, they deliver similar discharge capacity (1300 mAh g^{-1}) in the first cycle, but very different charge capacity (892 mAh g^{-1} for SnO-C; 729 mAh g^{-1} for SnO-B; 567 mAh g^{-1} for SnO-S). This demonstrates that SnO-C has more excellent Li-ion insertion/extraction ability, which contributes to its enhanced electrochemical properties.

Fig. 5*a* shows the cycling performance of the SnO-C, SnO-B, and SnO-S at 50 mA g^{-1}. All tested electrodes undergo sharply decrease during the first 30 cycles then nearly keep stable, which ascribes to the pulverisation of electrodes. At 80 cycles,

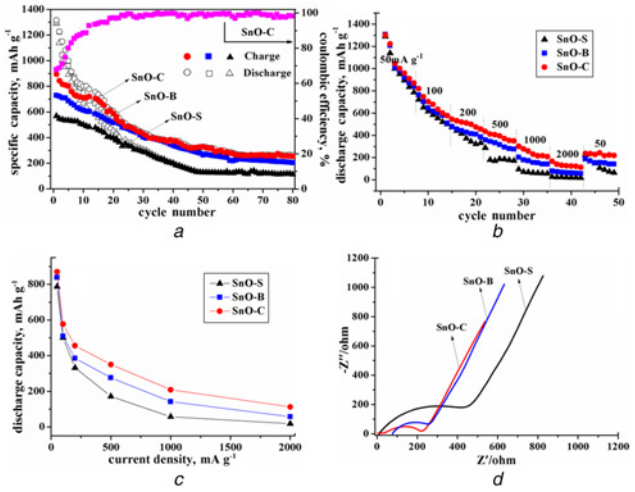

Fig. 5 *Electrochemical performances of*
a Cycling behaviour of the SnO-C, SnO-B, and SnO-S at 50 mA g^{-1}
b Rate performance of the SnO-C, SnO-B, and SnO-S electrodes at varied current densities
c Discharge capacity retention of the SnO-C, SnO-B, and SnO-S electrodes at 100, 200, 500, 1000, and 2000 mA g^{-1}
d Nyquist plots of EIS of the SnO-C, SnO-B, and SnO-S electrodes tested after 80 charge/discharge cycles

the SnO-C electrode delivers a reversible capacity of about 262 mAh g^{-1}, displaying higher capacity than SnO-B (203 mAh g^{-1}). While SnO-S electrode exhibits only 112 mAh g^{-1} after 80 cycles. Rate performance of the SnO-C, SnO-B, and SnO-S was evaluated in Fig. 5*b*. It is clear that SnO-B shows the highest discharge capacity among the three electrodes at various current densities. As shown in Fig. 5*c*, the SnO-C electrode can deliver a discharge capacity of 870, 576, 455, 350, 208, and 112 mAh g^{-1} at the current density of 50, 100, 200, 500, 1000, and 2000 mA g^{-1}, respectively, which is higher than that of SnO-B and SnO-S electrodes. When the rate is reset to 50 mA g^{-1} after 42 cycles, the capacity of SnO-C electrode recovers to some extent, to about 220 mAh g^{-1}, is indicating the good rate capability of SnO-C electrode. To understand the difference in electrochemical performance among SnO-C, SnO-B, and SnO-S electrodes, an EIS was measured shown in Fig. 5*d*. All the curves consist of a depressed semicircle in the high-medium frequency region and an inclined line in the low frequency region. Generally, the diameter of the semicircle represents the charge transfer impedance (*Rct*), which is generated by the Li-ion transfer between the electrolyte and the working electrode surface [35]. It is obvious that the *Rct* of SnO-C is smaller than that of SnO-B and SnO-S, indicating the diffusion of Li ions in the SnO-C electrode is rather easier. Combined with the electrochemical test results, we can conclude that the SnO-C electrode presents higher capacity, better cycling stability and smaller Rct value in comparison with the SnO-B and SnO-S electrodes. This could be related to the structural stability of SnO-C electrode, which can be understood by SEM analysis after cycles.

The cycled SnO electrodes with different morphology were examined by SEM analysis at the fully charged state. As shown in Fig. 6*a*, the crossed-like structure of SnO-C has changed into several microspheres with many particles assembled, indicating that the crossed-like SnO could maintain its original morphology to some extent. This could provide a reasonable explanation for the cycling stability of SnO-C. While SnO with block (SnO-B) and shell (SnO-S) structures present collapsed and agglomerated morphology, showing poor structural stability. The agglomerated morphology may hinder the charge transfer in the electrode and lead to more inferior cycling stability to SnO-C. Based on the above experimental results, the difference of electrochemical performance among SnO-C, SnO-B, and SnO-S could ascribe to size, crystallinity and structural stability. SnO-C electrode shows smaller particle size and higher crystallinity in comparison with SnO-B and SnO-S. The small size could shorten

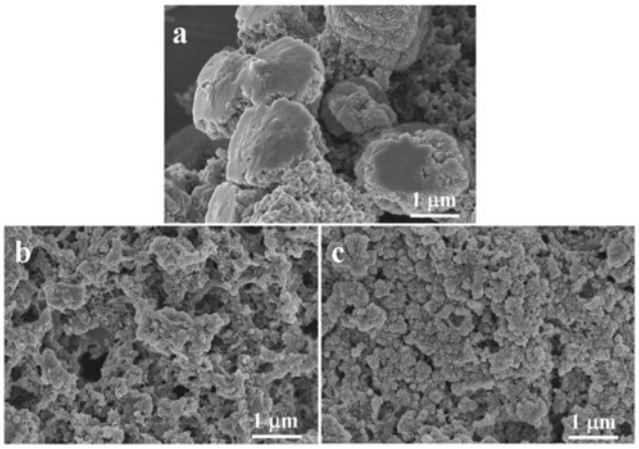

Fig. 6 *SEM images of*
a SnO-C
b SnO-B and
c SnO-S electrodes after 80 cycles

the diffusion paths of Li^+ in the electrode and high crystallinity with the atomic structure arranged regularly facilitates the fast transfer of Li^+ and electron. In addition, the stable structure is beneficial to obtain long-term cycling stability. Therefore, we conclude that small particle size, high crystallinity, and good structural stability are more advantageous to obtain enhanced electrochemical performance.

4. Conclusions: In summary, the pure phase of SnO with crossed, block, and shell like structures was prepared by a simple hydrothermal method. The electrochemical performance of the SnO with various structures was obtained by galvanostatic charge–discharge measurements. It is found that the cycling and rate properties of the crossed SnO are superior to that of the block and shell-like SnO. The first reversible capacity of crossed SnO could reach to 892 mAh g^{-1} at a current density of 50 mA g^{-1} and the capacity of 262 mAh g^{-1} can be still kept after 80 cycles. Even tested at 2000 mA g^{-1}, the crossed SnO could deliver a discharge capacity of 112 mAh g^{-1}. This superior electrochemical performance is ascribed to the unique crossed morphology with small particle size, high crystallinity, and good structural stability. These results suggest that the morphology and particle size have a significant influence on the synthesis SnO electrode materials with enhanced performance.

5. Acknowledgements: This work was financially supported by the National Natural Science Foundation of China (grant no. 51672165), Innovation Team Assistance Foundation of Shaanxi Province (grant no. 2013KCT-06), Scientific Special Foundation of Shaanxi Province Office of Education (grant no. 15JK1074), 973 Special Preliminary Study Plan (grant no. 2014CB260411) and Graduate Innovation Fund of Shaanxi University of Science and Technology.

6 References

[1] Zhang L., Lu L., Zhang D.C., *ET AL.*: 'Dual-buffered SnSe@CNFs as negative electrode with outstanding lithium storage performance', *Electrochim. Acta*, 2016, **209**, pp. 423–429
[2] Zhang C.F., Chen Z.X., Guo Z.P., *ET AL.*: 'Additive-free synthesis of 3D porous V_2O_5 hierarchical microspheres with enhanced lithium storage properties', *Energy Environ. Sci.*, 2013, **6**, pp. 974–978
[3] Liu Y., Zhu M.Q., Chen D.: 'Sheet-like $MoSe_2$/C composites with enhanced Li-ion storage properties', *J. Mater. Chem. A*, 2015, **3**, pp. 11857–11862
[4] Luo L., Xu W.Z., Xia Z.K., *ET AL.*: 'Electrospun ZnO-SnO_2 composite nanofibers with enhanced electrochemical performance as lithium-ion anodes', *Ceram. Int.*, 2016, **42**, pp. 10826–10832
[5] Wang Y.K., Ding J., Liu Y.H., *ET AL.*: 'SnO_2@reduced graphene oxide composite for high performance lithium-ion battery', *Ceram. Int.*, 2015, **41**, pp. 15145–15152
[6] Zhang J., Ma Z.S., Jiang W.J., *ET AL.*: 'Sandwich-like CNTs@ SnO_2/SnO/Sn anodes on three-dimensional Ni foam substrate for lithium ion batteries', *J. Electroanal. Chem.*, 2016, **767**, pp. 49–55
[7] Jiang W.J., Zeng W.Y., Ma Z.S., *ET AL.*: 'Advanced amorphous nanoporous stannous oxide composite with carbon nanotubes as anode materials for lithium-ion batteries', *RSC Adv.*, 2014, **4**, pp. 41281–41286
[8] Chen B.B., Qian H., Xu J.H., *ET AL.*: 'Study on SnO_2/graphene composites with superior electrochemical performance for lithium-ion batteries', *J. Mater. Chem. A*, 2014, **2**, pp. 9345–9352
[9] Yamaguchi H., Nakanishi S., Iba H., *ET AL.*: 'Amorphous polymeric anode materials from poly (acrylic acid) and tin (II) oxide for lithium ion batteries', *J. Power Sources*, 2015, **275**, pp. 1–5
[10] Cheng Y.Y., Huang J.F., Li R.Z., *ET AL.*: 'Enhanced cycling performances of hollow Sn compared to solid Sn in Na-ion battery', *Electrochim. Acta*, 2015, **180**, pp. 227–233
[11] Chao S.-C., Yen Y.-C., Song Y.-F., *ET AL.*: 'In situ transmission X-ray microscopy study on working SnO anode particle of Li-ion batteries', *J. Electrochem. Soc.*, 2011, **158**, pp. A1335–A1339
[12] Shimizu M., Usui H., Sakaguchi H.: 'Electrochemical Na-insertion/extraction properties of SnO thick-film electrodes prepared by gas-deposition', *J. Power Sources*, 2014, **248**, pp. 378–382
[13] Guo Y.Q., Tan R.Q., Li X., *ET AL.*: 'Shape-controlled growth and single-crystal XRD study of submillimeter-sized single crystals of SnO', *CrystEngComm*, 2011, **13**, pp. 5677–5680
[14] Yue W.B., Yang S., Ren Y., *ET AL.*: 'In situ growth of Sn, SnO on graphene nanosheets and their application as anode materials for lithium-ion batteries', *Electrochim. Acta*, 2013, **92**, pp. 412–420
[15] Sakaushi K., Oaki Y., Uchiyama H., *ET AL.*: 'Aqueous solution synthesis of SnO nanostructures with tuned optical absorption behavior and photoelectrochemical properties through morphological evolution', *Nanoscale*, 2010, **2**, pp. 2424–2430
[16] Aurbach D., Nimberger A., Markovsky B., *ET AL.*: 'Nanoparticles of SnO produced by sonochemistry as anode materials for rechargeable lithium batteries', *Chem. Mater.*, 2002, **14**, pp. 4155–4163
[17] Wang Z.L., Pan Z.W.: 'Junctions and networks of SnO nanoribbons', *Adv. Mater.*, 2002, **14**, pp. 1029–1032
[18] Sakaushi K., Oaki Y., Uchiyama H., *ET AL.*: 'Synthesis and applications of SnO nanosheets: parallel control of oxidation state and nanostructure through an aqueous solution route', *Small*, 2010, **6**, pp. 776–781
[19] Sun G., Qi F.X., Li Y.W., *ET AL.*: 'Solvothermal synthesis and characterization of ultrathin SnO nanosheets', *Mater. Lett.*, 2014, **118**, pp. 69–71
[20] Kumar B., Lee D.-H., Kim S.-H., *ET AL.*: 'General route to single-crystalline SnO nanosheets on arbitrary substrates', *J. Phys. Chem. C*, 2010, **114**, pp. 11050–11055
[21] Hu Y.J., Xu K.X., Kong L.Y., *ET AL.*: 'Flame synthesis of single crystalline SnO nanoplatelets for lithium-ion batteries', *Chem. Eng. J.*, 2014, **242**, pp. 220–225
[22] Iqbal M.Z., Wang F.P., Zhao H.L., *ET AL.*: 'Structural and electrochemical properties of SnO nanoflowers as an anode material for lithium ion batteries', *Scr. Mater.*, 2012, **67**, pp. 665–668
[23] Yang Y.C., Liu J., Li C., *ET AL.*: 'Fabrication of pompon-like and flower-like SnO microspheres comprised of layered nanoflakes by anodic electrocrystallization', *Electrochim. Acta*, 2012, **72**, pp. 94–100
[24] Dai Z.R., Pan Z.W., Wang Z.L.: 'Growth and structure evolution of novel tin oxide diskettes', *J. Am. Chem. Soc.*, 2002, **124**, pp. 8673–8680
[25] Wang L., Ji H.M., Zhu F., *ET AL.*: 'Large-scale preparation of shape controlled SnO and improved capacitance for supercapacitors: from nanoclusters to square microplates', *Nanoscale*, 2013, **5**, pp. 7613–7621
[26] Cui Y.K., Wang F.P., Iqbal M.Z., *ET AL.*: 'Synthesis of nanoflakes-based self-assembling crossed structure of stannous oxide and photocatalysis property', *Cryst. Res. Technol.*, 2015, **50**, pp. 210–214
[27] Iqbal M.Z., Wang F.P., Feng T., *ET AL.*: 'Facile synthesis of self-assembled SnO nano-square sheets and hydrogen absorption characteristics', *Mater. Res. Bull.*, 2012, **47**, pp. 3902–3907
[28] Ning J.J., Jiang T., Men K.K., *ET AL.*: 'Syntheses, characterizations, and applications in lithium ion batteries of hierarchical SnO nanocrystals', *J. Phys. Chem. C*, 2009, **113**, pp. 14140–14144
[29] Cheng Y.Y., Huang J.F., Li J.Y., *ET AL.*: 'Structure-controlled synthesis and electrochemical properties of $NH_4V_3O_8$ as cathode material for lithium ion batteries', *Electrochim. Acta*, 2016, **212**, pp. 217–224
[30] Bi Z.Y., Zhang X.D., He W., *ET AL.*: 'Recent advances in $LiFePO_4$ nanoparticles with different morphology for high-performance lithium-ion batteries', *RSC Adv.*, 2013, **3**, pp. 19744–19751
[31] Wang L., Ji H.M., Wang S.S., *ET AL.*: 'Preparation of Fe_3O_4 with high specific surface area and improved capacitance as a supercapacitor', *Nanoscale*, 2013, **5**, pp. 3793–3799
[32] Guan B.Y., Yu L., Li J., *ET AL.*: 'A universal cooperative assembly-directed method for coating of mesoporous TiO_2 nanoshells with enhanced lithium storage properties', *Sci. Adv.*, 2016, **2**, pp. 1–8
[33] Zhang H.J., He Q.Q., Wei F.J., *ET AL.*: 'Ultrathin SnO nanosheets as anode materials for rechargeable lithium-ion batteries', *Mater. Lett.*, 2014, **120**, pp. 200–203
[34] Uchiyama H., Hosono E., Honma I., *ET AL.*: 'A nanoscale meshed electrode of single-crystalline SnO for lithium-ion rechargeable batteries', *Electrochem. Commun.*, 2008, **10**, pp. 52–55
[35] Zhang H., Liu X.J., Wang R.L., *ET AL.*: 'Coating of α-MoO_3 on nitrogen-doped carbon nanotubes by electrodeposition as a high-performance cathode material for lithium-ion batteries', *J. Power Sources*, 2015, **274**, pp. 1063–1069

doi: 10.1049/mnl.2017.0550